General rule for the energy of water-induced traps in organic semiconductors

Guangzheng Zuo, Mathieu Linares, Tanvi Upreti and Martijn Kemerink

The self-archived postprint version of this journal article is available at Linköping University Institutional Repository (DiVA):
http://urn.kb.se/resolve?urn=urn:nbn:se:liu:diva-158312

N.B.: When citing this work, cite the original publication.
The original publication is available at www.springerlink.com:
Zuo, G., Linares, M., Upreti, T., Kemerink, M., (2019), General rule for the energy of water-induced traps in organic semiconductors, *Nature Materials*, 18(6), 588-+.
https://doi.org/10.1038/s41563-019-0347-y

Original publication available at:
https://doi.org/10.1038/s41563-019-0347-y
Copyright: Nature Research (part of Springer Nature)
http://www.nature.com/

Tweet

LINKÖPING UNIVERSITY

General Rule for the Energy of Water-Induced Traps in Organic Semiconductors

*Guangzheng Zuo[1], Mathieu Linares[2,3,4], Tanvi Upreti[1] and Martijn Kemerink[1]**

[1]Complex Materials and Devices, Department of Physics, Chemistry and Biology, Linköping University, 58183 Linköping, Sweden

[2]Laboratory of Organic Electronics, ITN, Linkoping University, SE-581 83 Linköping, Sweden

[3]Scientific Visualization Group, ITN, Linköping University, SE-581 83 Linköping, Sweden

[4]Swedish e-Science Research Centre (SeRC), Linköping University, SE-581 83 Linköping, Sweden

Charge carrier traps are generally highly detrimental for the performance of semiconductor devices. Unlike the situation for inorganic semiconductors, detailed knowledge about the characteristics and causes of traps in organic semiconductors is still very limited. Here, we accurately determine hole and electron trap energies for a wide range of organic semiconductors in thin-film form. We find that electron and hole trap energies follow a similar empirical rule and lie ~0.3 – 0.4 eV above (below) the highest occupied and lowest unoccupied molecular orbitals, respectively. Combining experimental and theoretical methods, the origin of the traps is shown to be a dielectric effect of water penetrating nano-voids in the organic semiconductor thin film. We also propose a solvent-annealing method to remove water-related traps from the materials investigated, irrespective of their energy levels. These findings represent a step towards the realization of trap-free organic semiconductor thin films.

Keywords: organic semiconductors; trapping; charge transport; water; QM/MM

Organic semiconductors, that is conjugated polymers (CPs) and small molecules, have been studied intensively as promising active materials for applications like organic solar cells, light-emitting diodes (LED) and electrochemical cells, field-effect transistors (FET), memories, sensors and so on.[1–6] For all these applications, the presence in the active material of charge carrier traps, being localized states in the semiconductor bandgap, is a known factor that heavily deteriorates performance.[7–15] For instance, it has been argued that the presence of a specific electron trap is the main reason for the typically lower electron mobility in many CPs.[9,16] In polymer-based LEDs, the imbalance of carrier mobilities caused by traps is a major cause for the loss in quantum efficiency.[17] In organic solar cells and LEDs, traps are known to cause non-radiative Shockley-Read-Hall recombination, decreasing the quantum efficiency.[18–22]

Unfortunately, there is still a limited fundamental understanding of traps in organic semiconductors, both in terms of their distribution in energy and in terms of the underlying physical causes. Proposed causes include conformational defects from twists and kinks in the polymer backbone, synthetic defects, impurities remaining from solvents and synthesis, contamination from the processing or ambient environment etc.[23–25] Alternatively, the presence of water in various guises in conjugated polymers has been suggested as the cause of predominantly electron traps[9,26], but also of hole traps.[10,27]

Although surprisingly few systematic investigations to the energetics of traps in organic semiconductors have been conducted, electron-only diodes based on a wide range of CPs were investigated in Ref. [9] and it was concluded that the electron trap level was about constant and centered at an energy of ~3.6 eV below the vacuum level. The common origin was argued to be most likely related to hydrated oxygen complexes. Alternatively, hole trapping in high-performance p-type organic FETs was attributed to water incorporated in nanometer-sized voids within the disordered CP microstructure.[10] The mechanism was proposed to be a hydrogen bonding interaction of a single water molecule water affecting the torsional potential energy profile of the bond connecting the donor and acceptor subunits of the polymer, causing the formation of shallow traps.

Here, we systematically investigate the current density vs applied voltage (JV) characteristics from both hole- and electron-only thin-film devices for a large range of organic semiconductors. Trap energies and densities are extracted directly from the JV curves and, more accurately, using a method based on the logarithmic slope of the JV curves. The two methods yield consistent results. For all investigated materials, the hole and electron trap distributions are found to be centered at a more or less constant energy offset of 0.3–0.4 eV above the highest occupied molecular orbital (HOMO) and below the lowest unoccupied molecular orbital (LUMO) level, respectively. For typical preparation and measurement conditions the total trap density is around $0.5–1\times10^{23}$ m^{-3} for both electrons and holes. We experimentally identify water absorbed in nano-voids as cause. Using density functional theory (DFT) calculations we show that direct interaction of H_2O molecules with the conjugated backbone cannot explain specific conformation locks nor the finding of a generic trap. Instead, we show that electrostatic interaction with an ensemble of H_2O molecules that for example are enclosed in a nanoscopic void in the film provides a stabilization of both electron and hole polarons on different model systems of conjugated molecule. The mechanism has a broad relevance as it does not rely on

any specific interactions with, or properties of the active material like conjugation length, mobility or transport mechanism, and is shown to affect electron and hole transport in a similar manner. The prerequisite of having nano-voids in the molecular morphology suggests this trapping mechanism to be of lesser relevance for single crystals, but also suggests processing routes to suppress the mechanism; an example of the latter is demonstrated.

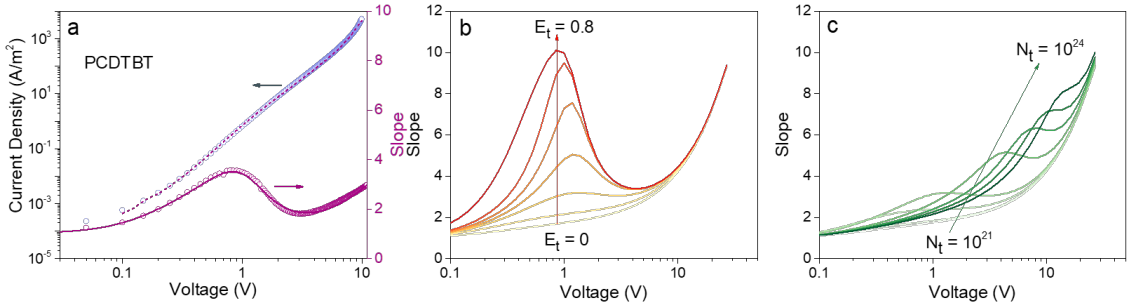

Figure 1 | Analysis of current-voltage characteristics. a, Experimental (dots) and simulated (lines) current density and slope vs voltage curves of PCDTBT (162 nm). Model parameters: E_t = 0.35 eV, N_t = 1×10^{23} m^{-3} and σ_{DOS} = 0.12 eV (JV-fit, dashed line) and E_t = 0.40 eV, N_t = 6×10^{22} m^{-3} and σ_{DOS} = 0.10 eV (slope-fit, solid line). **b**, Calculated slope vs voltage curves with varying E_t = 0 to 0.8 eV (orange to red) at a constant N_t = 1×10^{23} m^{-3} and **c**, varying N_t = 10^{21} to 10^{24} m^{-3} (light to dark green) at a constant E_t = 0.3 eV. Other parameters: inter-site distance α_{NN}= 1.8 nm; thickness = 100 nm; σ_{DOS} = 0.075 eV; temperature T = 300 K.

We fabricated hole- and electron-only devices with the structure of ITO/PEDOT:PSS/active layer/MoO_3/Al and Al/active layer/$CsCO_3$/Al, respectively; the latter is deliberately the same as in Ref.[9], except for the $CsCO_3$ that we found to be a better electron injecting contact than Ba/Al.[28] Further experimental details and the full names as well as the chemical structure and energy levels of the materials used can be found in the Methods section and Section S1 of the Supplementary Information (SI). As an example, Figure 1a shows the JV curve of a PCDTBT hole-only device. The double-log representation shows a weak hump in the JV curve around 1 V. In previous works, we have shown how the logarithmic slope of JV curves, $slope = d(log\ j)/d(log\ V)$, can reveal the presence of energetic traps.[29,30] In this case, the hump in the JV curve translates into a distinct peak in the slope curve and indicates a transition between low-conductivity trap-limited and high-conductivity trap-filled charge transport regimes.[31] In other words, the peak highlights the trap-filling regime. Indeed, the slope curve, red symbols in Figure 1a, show a pronounced peak at low bias.

To quantitatively interpret the JV and slope curves, and in particular to extract the position and energetic distribution of the traps, we developed a 1D drift-diffusion model.[29] In brief, the model solves the coupled drift-diffusion, continuity and Poisson equations, using parametrized mobility functionals to account for energetic disorder.[32] Following Nicolai, traps are assumed to be normally distributed with a width that is equal to the Gaussian disorder of the HOMO or LUMO level.[9,33] Their filling is described using the expressions developed in Ref. [34]. Injection barrier lowering by the image potential is accounted for.[35] The model clearly reproduces the slope curve including the peak around 1 V applied bias, see the solid line in Figure 1; the used

parameters are given in the caption. Note that the peak cannot be reproduced without including a (broadened) trap level. In particular, it can be ruled out that the peak results from a finite built-in voltage or other effects of non-negligible injection barriers as discussed in detail in the SI, section S2. Figures 1b and c show calculated slope curves that illustrate how trap depth and trap density have orthogonal effects on the peak in affecting predominantly its height and its position, respectively. Hence, both depth and density can be determined with good accuracy from the measured peak. Alternatively, we used the same method as Ref. [9] to derive these parameters by directly fitting the JV curves, see the dashed line in Figure 1a. While both methods yield consistent results, we find the slope-fitting procedure to be more precise than JV curve fitting. The simple reason is that the former focusses on the region that is dominated by the trap-filling process, while JV curve fitting strongly depends on choosing the correct bias range and is more sensitive to the choice of the other transport parameters, particularly the Gaussian disorder, inter-site distance and injection barrier height. In contrast, the slope-fitting method is almost independent on those parameters as shown in the SI section S3. Note, finally, that the continuous increase in slope at high voltages in the trap-filled regime reflects mobility increases due to the increasing electric field and charge density.[32]

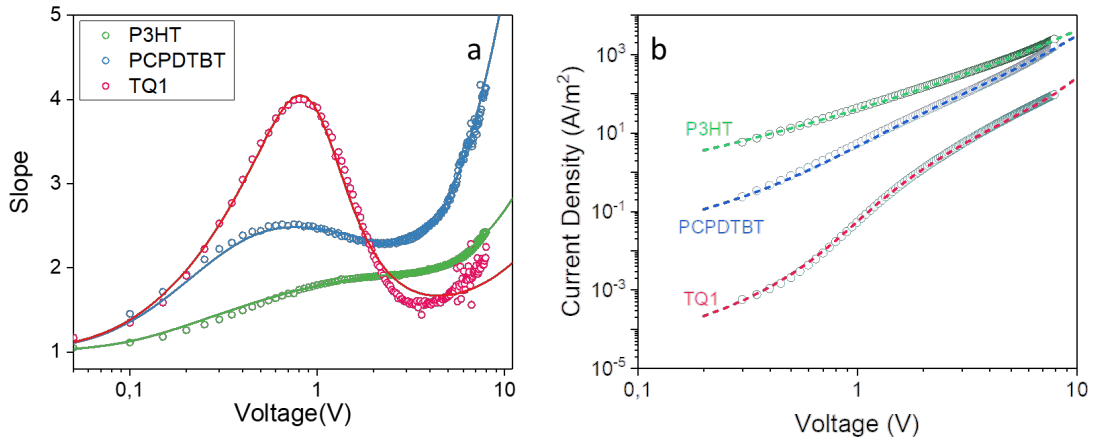

Figure 2 | current-voltage characteristics of hole-only devices. a. Slope vs voltage curves from hole-only devices (dots) and model fits (solid lines) for P3HT (286 nm, E_t = 0.15 eV, N_t = 1×10^{23} m^{-3} and σ_{DOS} = 0.05 eV, green); PCPDTBT (210 nm, E_t = 0.32 eV, N_t = 6×10^{22} m^{-3} and σ_{DOS} = 0.08 eV, blue); and TQ1 (298 nm, E_t = 0.43 eV, N_t = 5.2×10^{22} m^{-3} and σ_{DOS} = 0.10 eV, red). **b**. Corresponding JV curves from hole-only devices (dots) and model fits (dashed lines) for P3HT (E_t = 0.1±0.05 eV, N_t =1×10^{23} m^{-3} and σ_{DOS} = 0.05 eV, green); PCPDTBT (E_t = 0.32 ± 0.05 eV, N_t = 5×10^{22} m^{-3} and σ_{DOS} = 0.08 eV, blue); and TQ1 (E_t = 0.40 ± 0.05 eV, N_t = 6×10^{22} m^{-3} and σ_{DOS} = 0.11 eV, red).

To investigate the presence of systematic trends in trap energies in organic semiconductors, we chose a wide range of materials with the HOMO running from -5.0 to -6.0 eV and LUMO from -3.0 to -4.0 eV and measured their JV characteristics. P3HT, PCPDTBT and TQ1 have a HOMO energy level of -5.0, -5.3 and 5.7 eV, respectively. Each of them displays a distinct peak in the slope vs voltage curve in Figure 2a that becomes more pronounced with lower-lying

HOMO energy but that does not show any systematic shifts. In view of the discussion of Figure 1b above, the behavior can be attributed to increasingly deep traps of an almost constant density. Explicit analysis using our model confirmed this interpretation. The hole-only JV curves not shown in the main text and their analysis are shown in the SI, section S4. The same holds for the electron-only curves that are shown in section S5

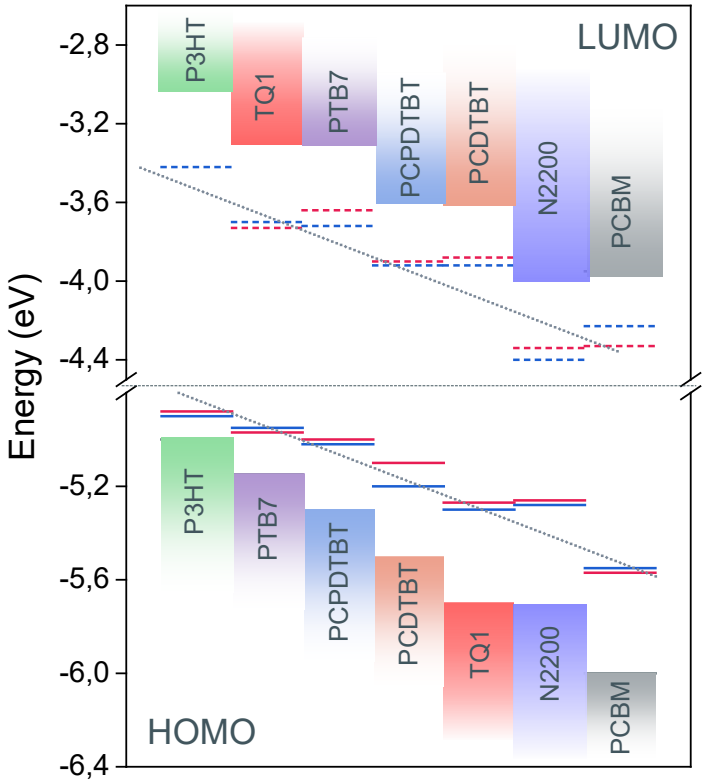

Figure 3 | Electron and hole trap energies. Hole (solid lines) and electron (dashed lines) trap energies in relation to HOMO (shaded area on bottom) and LUMO (top) energy levels for the investigated range of organic materials. Trap energies determined by slope- and JV-fitting are shown as red and blue lines, respectively. The thin black dotted lines are guides to the eye.

For the used preparation and measurement conditions, the total density of hole and electron traps is around $0.5–1\times10^{23}$ m^{-3} for all materials, see Tables S1 and S2 in the SI. Figure 3 summarizes the trap energies from both slope- and JV-fitting. Clearly, neither the hole nor the electron trap energies are constant. Instead, both shift down with lower-lying HOMO or LUMO energy level. For holes, shallower HOMO levels seem to give rise to shallower traps, confirming the trend discussed at Figure 2 above. For electrons, such systematic behavior seems absent and the electron trap appears to be located at a more or less constant offset of 0.3–0.4 eV below the LUMO energy.

Although N2200 and the small molecule PCBM are commonly considered good electron transporting materials, they form no exception to the general rule for n-type traps found in Figure 3. The measured zero-field, zero-density electron mobility values of $\mu_{0,e}$ = 1.2×10^{-7}

m^2/Vs and 6×10^{-7} m^2/Vs for N2200 and PCBM are consistent with earlier findings, ruling out the possibility that we somehow measured degraded devices. Instead, finding a trap level that shifts with HOMO or LUMO level of the semiconductor points at another mechanism than an oxidative or reductive reaction with a specific compound that would lead to a more or less constant trap energy. This generic mechanism would come on top of any such specific reactions. Hence, while the deep LUMO of both N2200 and PCBM would protect these compounds from oxidative reactions with H_2O,[26] they would still be susceptible to this generic and so far unknown mechanism.

Inspired by the findings in Refs. [10,29], we suggest as a possible mechanism the dielectric effect of water-filled nanoscopic voids in the disordered morphology of the active layer. It is well-known from ultra-high vacuum technology that traces of water, especially on surfaces, cannot be removed from a system without bake-out at temperatures much above 100 °C. Hence, in a glovebox, even at <1 ppm H_2O, there is sufficient water present to almost instantaneously penetrate any thin film device. As trapping mechanism, we propose the stabilization of 'any' charged species, specifically a polaron, by an ensemble of (dipolar) water molecules sitting in its vicinity. This dielectric effect will, in lowest order, not depend on the energy level in which the charge sits, nor on its polarity, in line with the observations in Figure 3.

To experimentally determine whether indeed minute traces of water are somehow involved in the observed trap formation, we repeated the JV measurements for selected devices that were subjected to either a thermal annealing step in dry N_2 atmosphere or a solvent annealing step in saturated o-xylene atmosphere, see Figure 4. For both hole- and electron-only devices the steady-state current density at low bias is increased by the thermal annealing step prior to contact deposition, accompanied by a slight suppression of the trapping peak in the corresponding slope plot, see red and blue curves in panel a. While being consistent with the notion that water is involved in the trapping process, the minor effect of dry annealing on trapping suggests that either incomplete removal or, more likely, reuptake or of water limits the effectiveness of this processing step. In stark contrast, the effect of solvent annealing is much stronger, leading to a complete (holes) or almost complete (electrons) removal of the trapping peak and a significant increase in current density (green curves). This observation is consistent with a scenario in which a compacting, morphological rearrangement of the semiconductor material removes the (majority of the) nano-voids during solvent annealing. This both dries the film and, in contrast to dry annealing, prevents the reuptake of water. A schematic illustration of the proposed mechanism is given in Figure 4b.

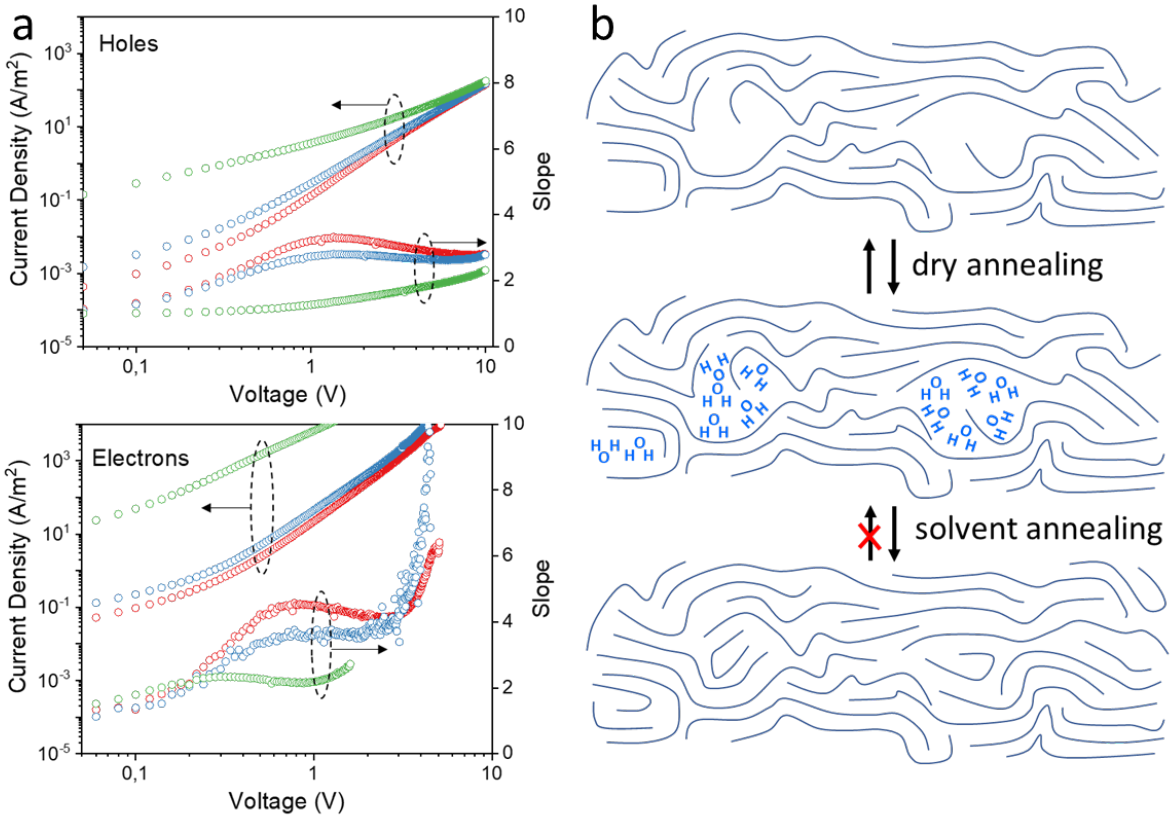

Figure 4 | Impact of thermal and solvent treatment on traps. a. current density and slope vs voltage curves from hole-only (upper) and electron-only (bottom) TQ1 devices, as-cast (red), after thermal annealing (blue) and after solvent annealing (green). **b.** Schematic illustration of the effect of dry annealing and solvent annealing, with only the latter leading to the compacting of the pristine semiconductor film (middle panel), leading to the removal of the (majority of the) water-filled nano-voids acting as generic charge trap.

The results in Figure 4 show that, although other sources of traps are likely to be present, the water-induced trap is the by far dominant one in the pristine active layer. After solvent annealing any remaining hole (electron) traps have a density below (at about) our experimental detection limit of ~1×10^{22} m^{-3}. Although this topic will not be further pursued here, we also note that after solvent annealing the electron current density in the 'p-type' polymer TQ1 is actually higher than that of the holes by about two orders of magnitude, which is also reflected in the extracted zero-field, zero-density mobility values of $\mu_{0,h}$ = 7.7×10^{-10} m^2/Vs and $\mu_{0,e}$ = 2.2×10^{-7} m^2/Vs for the solvent-annealed device. This finding is consistent with recent work on organic thermoelectrics and on organic solar cells that both suggest that the trap-free mobility of electrons may be higher than that of holes in one and the same material.[36,37]

Using DFT calculations (see Methods) we first attempted to produce a generic trap by placing a water molecule in close proximity of model oligomers and investigating the resulting changes in electron affinity and ionization potential.[9,10] As discussed in the introduction section, it was previously proposed that water molecules around the polymer could lock it in a specific conformation and thereby create a generic trap.[10] However, in our case we were not able to

identify a generic trap but observe that both stabilization and destabilization of the hole or electron polaron can occur and that these processes are extremely dependent on the conformation considered. Full details are given in SI section S6.

To test the hypothesis that charge trapping instead is caused by dielectric effects from nano-inclusions of water in the semiconductor film, we performed QM/MM calculations on model systems consisting of either a thiophene or thiophene-quinoxaline oligomer (6T or 3TQ) with a water nano-droplet of increasing size around it; SI section S7 provides full details. In our calculations, the oligomer is treated at the QM level while the water molecules are represented as polarizable point charges (See Methods). As expected on basis of the unspecific (electrostatic) interaction mechanism, the general trend is that both electron and hole polarons are stabilized, irrespective of the conjugated compound containing a single repeat unit (6T) or being of donor-acceptor type (3TQ). Likewise, the mechanism will apply to polymers, oligomers and small molecules in a similar fashion, and irrespective of mobility or transport mechanism. The stabilization, that is the trap formation, increases with droplet size and corresponds to trap depths ~0.3–0.5 eV that are entirely consistent with the experimental observations in Figure 3, see also SI figure 10. We note that for 6T, the stabilization of the electron polaron by the water nanodroplet is significantly stronger than for the hole polaron, in agreement with the experimental observations for P3HT in Figure 3; for 3TQ electron and hole polaron stabilizations are more similar, as is the case for TQ1. For the smallest droplets, fluctuations are observed which we attribute to the complete filling of successive hydration shells of water molecules around the center of the molecules; note also that the periodicity is equal for EA and IP.

The trap depths calculated above should be considered an upper limit that applies when the molecule is completely surrounded by water. In actual samples, a significant fraction of molecules will only on one side be exposed to the water droplet. We confirmed by explicit calculations, shown in SI figure 11, that also in this case a water-induced trap forms, with a depth that is only slightly lower than for full coverage. Although our model provides a semi-quantitative explanation for the depth of water-induced charge traps in conjugated semiconductors, it does not provide a straightforward rationalization for the observed narrow range of trap densities $0.5–1\times10^{23}$ m^{-3} for the samples treated using standard protocol. A detailed investigation of the dependency of E_t and N_t on preparation, measurement and storage history strongly suggests that the relative constancy of N_t to a significant degree reflects the nominally identical measurement conditions used for the measurements underlying figure 3. Unsurprisingly, N_t and, to a lesser degree (see figure 5), E_t depend on the amount of water that is present during active layer deposition and measurement, as discussed in more detail in SI section 8.

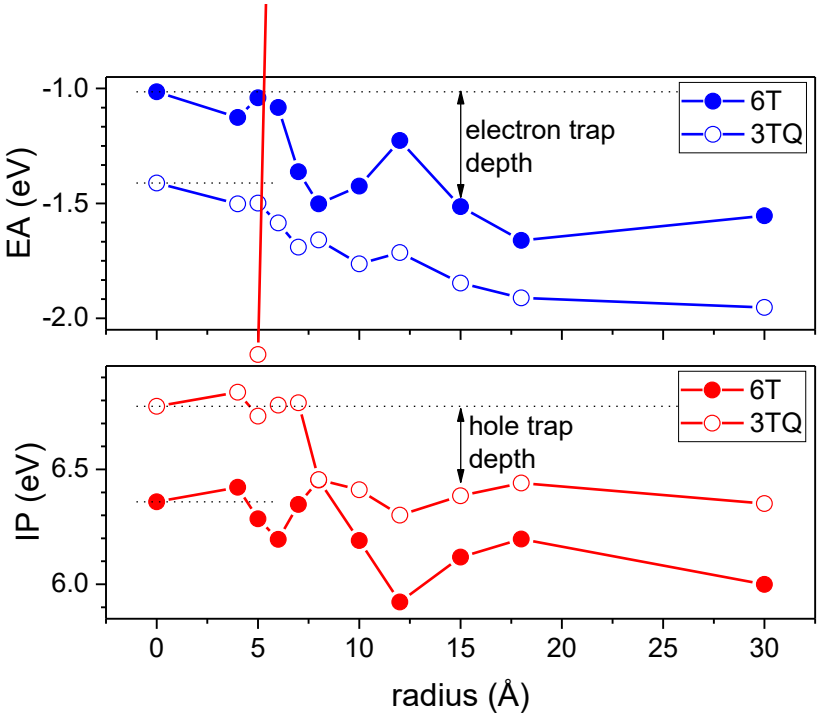

Figure 5 | Evolution of IP and EA with water nanodroplet size. Electron affinity (EA, blue)) and ionization potential (IP, red) as calculated by QM/MM for a 6T (solid lines) or a 6TQ (dashed lines) oligomer with a nano-droplet of water of the indicated radius at its center. Zero radius corresponds to vacuum.

In conclusion, we have shown the presence of electron and hole traps in thin-film devices based on a wide range of conjugated polymer semiconductors as well as in the conjugated small molecule PCBM. The trap level sits ~0.3–0.4 eV away from the HOMO (for holes) or LUMO (for electrons) level; for holes the trap gets shallower with shallower HOMO, a similar correlation could not be established for electrons. By combining the results from additional processing steps and ab-initio modeling, we could attribute the charge trapping to a universal, dielectric effect of nano-inclusions of water in the semiconductor thin film. The trap concentration therefore depends critically on preparation, storage and measurement conditions.

While suitable positioning of especially the LUMO level of conjugated materials with respect to the water and oxygen reduction levels is known to suppress trap formation through redox reactions, our results imply that fully trap-free conjugated materials can only be achieved by complete avoidance of even minute amounts of water. Compacting of the semiconducting layer through solvent treatment appears to be a promising route towards water-tolerant devices based on conjugated semiconductors. Although we performed our experiments on single-carrier diodes, avoiding traps is of evident relevance to all organic devices in which charge transport plays a role, including LEDs, FETs and solar cells.

Acknowledgements

The research by G.Z. was supported by the Chinese Scholarship Council (CSC). ML thanks SeRC (Swedish e-Science Research Center) for funding and SNIC (Swedish National Infrastructure for Computing) for computing resources (SNIC 2018/3-554).

Author contributions

G.Z. made all devices and performed and analyzed all experiments. M.L. performed DFT and QM/MM simulations. T.U. performed the processing conditions study. M.K. wrote the drift-diffusion simulation software, conceived the idea and coordinated research. G.Z. and M.K. wrote the manuscript with input from M.L.

Additional information

Supplementary information is available in the online version of the paper. Reprints and permissions information is available online at www.nature.com/reprints. Correspondence and requests for materials should be addressed to M.K.

Competing financial interests

The authors declare no competing financial interests.

Data availability

The data and code that support the findings of this study are available from the corresponding author upon reasonable request.

References

1. Nielsen, C. B., Holliday, S., Chen, H.-Y., Cryer, S. J. & McCulloch, I. Non-Fullerene Electron Acceptors for Use in Organic Solar Cells. *Acc. Chem. Res.* **48,** 2803–2812 (2015).
2. Grimsdale, A. C., Leok Chan, K., Martin, R. E., Jokisz, P. G. & Holmes, A. B. Synthesis of Light-Emitting Conjugated Polymers for Applications in Electroluminescent Devices. *Chem. Rev.* **109,** 897–1091 (2009).

3. Reenen, S. van & Kemerink, M. Light-Emitting Electrochemical Cells: Mechanisms and Formal Description. in *Light-Emitting Electrochemical Cells* 3–45 (Springer, Cham, 2017). doi:10.1007/978-3-319-58613-7_1
4. Zhao, Y., Guo, Y. & Liu, Y. 25th Anniversary Article: Recent Advances in n-Type and Ambipolar Organic Field-Effect Transistors. *Adv. Mater.* **25,** 5372–5391 (2013).
5. Asadi, K., Li, M., Blom, P. W. M., Kemerink, M. & de Leeuw, D. M. Organic ferroelectric opto-electronic memories. *Mater. Today* **14,** 592–599 (2011).
6. Torsi, L. *et al.* A sensitivity-enhanced field-effect chiral sensor. *Nat. Mater.* **7,** 412–417 (2008).
7. Abbaszadeh, D. *et al.* Elimination of charge carrier trapping in diluted semiconductors. *Nat. Mater.* **15,** 628–633 (2016).
8. Mandoc, M. M., de Boer, B., Paasch, G. & Blom, P. W. M. Trap-limited electron transport in disordered semiconducting polymers. *Phys. Rev. B* **75,** 193202 (2007).
9. Nicolai, H. T. *et al.* Unification of trap-limited electron transport in semiconducting polymers. *Nat. Mater.* **11,** 882–887 (2012).
10. Nikolka, M. *et al.* High operational and environmental stability of high-mobility conjugated polymer field-effect transistors through the use of molecular additives. *Nat. Mater.* **16,** 356–362 (2017).
11. Sirringhaus Henning. Reliability of Organic Field-Effect Transistors. *Adv. Mater.* **21,** 3859–3873 (2009).
12. Mandoc, M. M., Kooistra, F. B., Hummelen, J. C., de Boer, B. & Blom, P. W. M. Effect of traps on the performance of bulk heterojunction organic solar cells. *Appl. Phys. Lett.* **91,** 263505 (2007).
13. Blakesley, J. C. & Neher, D. Relationship between energetic disorder and open-circuit voltage in bulk heterojunction organic solar cells. *Phys. Rev. B* **84,** 075210 (2011).

14. Dittmer J. J., Marseglia E. A. & Friend R. H. Electron Trapping in Dye/Polymer Blend Photovoltaic Cells. *Adv. Mater.* **12,** 1270–1274 (2000).
15. Shao, Y., Xiao, Z., Bi, C., Yuan, Y. & Huang, J. Origin and elimination of photocurrent hysteresis by fullerene passivation in $CH_3NH_3PbI_3$ planar heterojunction solar cells. *Nat. Commun.* **5,** 5784 (2014).
16. Zhang, Y., de Boer, B. & Blom, P. W. M. Trap-free electron transport in poly(p-phenylene vinylene) by deactivation of traps with n-type doping. *Phys. Rev. B* **81,** 085201 (2010).
17. Tsai, M.-J. & Meng, H.-F. Electron traps in organic light-emitting diodes. *J. Appl. Phys.* **97,** 114502 (2005).
18. Kuik Martijn *et al.* 25th Anniversary Article: Charge Transport and Recombination in Polymer Light-Emitting Diodes. *Adv. Mater.* **26,** 512–531 (2014).
19. Kuik, M., Koster, L. J. A., Wetzelaer, G. A. H. & Blom, P. W. M. Trap-Assisted Recombination in Disordered Organic Semiconductors. *Phys. Rev. Lett.* **107,** 256805 (2011).
20. Wetzelaer, G. A. H., Kuik, M., Nicolai, H. T. & Blom, P. W. M. Trap-assisted and Langevin-type recombination in organic light-emitting diodes. *Phys. Rev. B* **83,** 165204 (2011).
21. Street, R. A., Schoendorf, M., Roy, A. & Lee, J. H. Interface state recombination in organic solar cells. *Phys. Rev. B* **81,** 205307 (2010).
22. Cowan, S. R., Roy, A. & Heeger, A. J. Recombination in polymer-fullerene bulk heterojunction solar cells. *Phys. Rev. B* **82,** 245207 (2010).
23. Graupner, W., Leditzky, G., Leising, G. & Scherf, U. Shallow and deep traps in conjugated polymers of high intrachain order. *Phys. Rev. B* **54,** 7610–7613 (1996).

24. Meier, M., Karg, S., Zuleeg, K., Brütting, W. & Schwoerer, M. Determination of trapping parameters in poly(p-phenylenevinylene) light-emitting devices using thermally stimulated currents. *J. Appl. Phys.* **84,** 87–92 (1998).
25. P. Nikiforov, M. *et al.* Detection and role of trace impurities in high-performance organic solar cells. *Energy Environ. Sci.* **6,** 1513–1520 (2013).
26. de Leeuw, D. M., Simenon, M. M. J., Brown, A. R. & Einerhand, R. E. F. Stability of n-type doped conducting polymers and consequences for polymeric microelectronic devices. *Synth. Met.* **87,** 53–59 (1997).
27. Gomes, H. L., Stallinga, P., Cölle, M., de Leeuw, D. M. & Biscarini, F. Electrical instabilities in organic semiconductors caused by trapped supercooled water. *Appl. Phys. Lett.* **88,** 082101 (2006).
28. Huang, J., Xu, Z. & Yang, Y. Low-Work-Function Surface Formed by Solution-Processed and Thermally Deposited Nanoscale Layers of Cesium Carbonate. *Adv. Funct. Mater.* **17,** 1966–1973
29. Zuo, G. *et al.* Molecular Doping and Trap Filling in Organic Semiconductor Host–Guest Systems. *J. Phys. Chem. C* **121,** 7767–7775 (2017).
30. Felekidis, N., Melianas, A. & Kemerink, M. Automated open-source software for charge transport analysis in single-carrier organic semiconductor diodes. *Org. Electron.* **61,** 318–328 (2018).
31. Mark, P. & Helfrich, W. Space-Charge-Limited Currents in Organic Crystals. *J. Appl. Phys.* **33,** 205–215 (1962).
32. Pasveer, W. F. *et al.* Unified Description of Charge-Carrier Mobilities in Disordered Semiconducting Polymers. *Phys. Rev. Lett.* **94,** 206601 (2005).
33. Nicolai, H. T., Mandoc, M. M. & Blom, P. W. M. Electron traps in semiconducting polymers: Exponential versus Gaussian trap distribution. *Phys. Rev. B* **83,** 195204 (2011).

34. Paasch, G. & Scheinert, S. Charge carrier density of organics with Gaussian density of states: Analytical approximation for the Gauss–Fermi integral. *J. Appl. Phys.* **107,** 104501 (2010).

35. van der Holst, J. J. M. *et al.* Modeling and analysis of the three-dimensional current density in sandwich-type single-carrier devices of disordered organic semiconductors. *Phys. Rev. B* **79,** 085203 (2009).

36. Zuo, G., Li, Z., Wang, E. & Kemerink, M. High Seebeck Coefficient and Power Factor in n-Type Organic Thermoelectrics. *Adv. Electron. Mater.* **4,** 1700501 (2017).

37. Melianas, A. *et al.* Photogenerated Carrier Mobility Significantly Exceeds Injected Carrier Mobility in Organic Solar Cells. *Adv. Energy Mater.* **7,** 1602143 (2017).

38. M. J. Frisch, G. W. Trucks, H. B. Schlegel, G. E. Scuseria, M. A. Robb, J. R. Cheeseman, G. Scalmani, V. Barone, B. Mennucci, G. A. Petersson, H. Nakatsuji, M. Caricato, X. Li, H. P. Hratchian, A. F. Izmaylov, J. Bloino, G. Zheng, J. L. Sonnenberg, M. Hada, M. Ehara, K. Toyota, R. Fukuda, J. Hasegawa, M. Ishida, T. Nakajima, Y. Honda, O. Kitao, H. Nakai, T. Vreven, J. A. Montgomery, Jr., J. E. Peralta, F. Ogliaro, M. Bearpark, J. J. Heyd, E. Brothers, K. N. Kudin, V. N. Staroverov, R. Kobayashi, J. Normand, K. Raghavachari, A. Rendell, J. C. Burant, S. S. Iyengar, J. Tomasi, M. Cossi, N. Rega, J. M. Millam, M. Klene, J. E. Knox, J. B. Cross, V. Bakken, C. Adamo, J. Jaramillo, R. Gomperts, R. E. Stratmann, O. Yazyev, A. J. Austin, R. Cammi, C. Pomelli, J. W. Ochterski, R. L. Martin, K. Morokuma, V. G. Zakrzewski, G. A. Voth, P. Salvador, J. J. Dannenberg, S. Dapprich, A. D. Daniels, Ö. Farkas, J. B. Foresman, J. V. Ortiz, J. Cioslowski, and D. J. Fox, Gaussian 09 (Gaussian, Inc., Wallingford CT, 2009). G09 | Gaussian.com.

39. Berendsen, H. J. C., van der Spoel, D. & van Drunen, R. GROMACS: A message-passing parallel molecular dynamics implementation. *Comput. Phys. Commun.* **91,** 43–56 (1995).

40. Lindahl, E., Hess, B. & van der Spoel, D. GROMACS 3.0: a package for molecular simulation and trajectory analysis. *Mol. Model. Annu.* **7,** 306–317 (2001).
41. Spoel, D. V. D. *et al.* GROMACS: Fast, flexible, and free. *J. Comput. Chem.* **26,** 1701–1718 (2005).
42. Jorgensen, W. L. & Tirado-Rives, J. The OPLS [optimized potentials for liquid simulations] potential functions for proteins, energy minimizations for crystals of cyclic peptides and crambin. *J. Am. Chem. Soc.* **110,** 1657–1666 (1988).
43. Jorgensen, W. L., Maxwell, D. S. & Tirado-Rives, J. Development and Testing of the OPLS All-Atom Force Field on Conformational Energetics and Properties of Organic Liquids. *J. Am. Chem. Soc.* **118,** 11225–11236 (1996).
44. Berendsen, H. J. C., Postma, J. P. M., van Gunsteren, W. F., DiNola, A. & Haak, J. R. Molecular dynamics with coupling to an external bath. *J. Chem. Phys.* **81,** 3684–3690 (1984).
45. DALTON: A Molecular Electronic Structure Program, Release DALTON2013.0. (2013).
46. Aidas, K. *et al.* The Dalton quantum chemistry program system. *Wiley Interdiscip. Rev. Comput. Mol. Sci.* **4,** 269–284 (2014).
47. Yanai, T., Tew, D. P. & Handy, N. C. A new hybrid exchange–correlation functional using the Coulomb-attenuating method (CAM-B3LYP). *Chem. Phys. Lett.* **393,** 51–57 (2004).
48. Kendall, R. A., Dunning, T. H. & Harrison, R. J. Electron affinities of the first-row atoms revisited. Systematic basis sets and wave functions. *J. Chem. Phys.* **96,** 6796–6806 (1992).
49. Woon, D. E. & Dunning, T. H. Gaussian basis sets for use in correlated molecular calculations. III. The atoms aluminum through argon. *J. Chem. Phys.* **98,** 1358–1371 (1993).

50. Ahlström, P., Wallqvist, A., Engström, S. & Jönsson, B. A molecular dynamics study of polarizable water. *Mol. Phys.* **68,** 563–581 (1989).

Methods

Fabrication – The active layers were spin-coated from a chloroform or o-dichlorobenzene solution in a dry nitrogen-filled glovebox with structure: ITO/PEDOT:PSS (40 nm)/active layer/MoO_3 (5 nm)/ Al (90 nm) for hole-only devices, and Al (90 nm)/active layer/$CsCO_3$ (2 nm)/Al (90 nm) for electron-only devices. Al bottom contacts and all top contacts were deposited by thermal evaporation through a shadow mask under high vacuum conditions. After spin coating the active layer, regular samples were directly loaded in the evaporator without contact to ambient. Two additional processing steps were applied to some samples: annealed samples were kept at 120°C for 30 minutes in the N_2 glovebox atmosphere before deposition of the top contact, solvent annealed samples were kept at 50 °C for 60 minutes in a saturated o-xylene atmosphere after deposition of the top contact.

Measurement – Current-voltage characteristics were measured directly after device fabrication inside the glovebox for electron-only devices. Hole-only devices were immediately measured outside the glovebox for convenience as we noticed no differences between devices measured in- and outside the glovebox. The JV curves shown in this work are all taken with the ITO/ PEDOT:PSS and the $CsCO_3$/Al contacts acting as hole- respectively electron-injecting contact.

DFT calculations on model systems – The different conformers were optimized at the ωB97Xd/6-31+G(d,p) level of theory, which allows a proper description of dispersion. The energy levels were then calculated at the more accurate level of theory MP2/6-311++G(d,p). The vertical electron affinity and ionization potential were calculated at the same level of theory. Calculations were performed with the Gaussian package.[38]

QM/MM calculations – The morphology to extract the model systems was obtained by solvating the model systems: (i) a chain of sexithiophene (6T); (ii) three repeating thiophene-quinoxaline units (3TQ) in water with a density of 1.0 g/cm^3. A short MD simulation of 300 ns was performed using the Gromacs package[39–41] in combination with the OPLS force-field[42,43] in the canonical ensemble at 300 K with the Berendsen thermostat[44] to ensure a reasonable position of the water molecules around the molecules. During this simulation the molecule were kept planar. From the final geometry of the simulation, models were created by including water molecules within an increasing radius of the central C-C bond. The number of water molecules and images of the different systems are presented in SI section S7. All quantum chemical response calculations were carried out with use of the Dalton program[45,46] employing Kohn−Sham density functional theory (DFT) in conjunction with the Coulomb attenuated B3LYP (CAM-B3LYP)[47] exchange correlation functional. For the solutes 6T and 3TQ, the aug-cc- pVDZ[48,49] basis set was used in all calculations, while for the surrounding water the polarizable MM potential of Ref.[50] was used.